Delay Spread Measurements for the Digital Cellular Channel in Toronto

Elvino S. Sousa, *Member, IEEE*, Vladan M. Jovanović, *Member, IEEE*, and Christian Daigneault, *Member, IEEE*

***Abstract*— This paper describes a set of measurements performed in the Toronto area, in order to assess the impact of multipath propagation on the performance of the TIA IS-54 digital standard. Five existing cells were systematically surveyed: two in downtown Toronto, two in the suburbs, and one in a suburban/rural area. A sweeping correlator apparatus with a 0.1 μs resolution and 910 MHz carrier frequency, and an omnidirectional antenna was used. In one of the cells, the measurements were repeated with a 60 degree beamwidth directional antenna. A fairly sophisticated *thresholding* technique was applied in order to reduce the impact of noise. Generally, the measurements with the omnidirectional antenna exhibit multipath propagation with considerably smaller excess delays than some reported recently, but are consistent with earlier results obtained in the U.S. and Europe. Sectorization was found to considerably reduce the multipath effects. Very large delay components appear to be due mostly to the combination of large transmitter–receiver distances and a large degree of shadowing, and could probably be avoided to a large extent by standard cellular engineering techniques. In view of these results, it seems that the long delay (high selectivity) problem has been somewhat overemphasized in the past, at least for areas like Toronto. Problems associated with short delays (flat fading), on the contrary, appear to have been underestimated in the case of dense urban environments.**

I. Introduction

THE CELLULAR radio industry is introducing new digital signaling schemes for mobile radio systems. The new techniques, based on narrow-band TDMA (North-American IS-54 standard), wide-band TDMA (European GSM), or CDMA, potentially offer a large increase in the channel capacity over current schemes utilizing analog FM modulation and FDMA. In general, however, these digital schemes are more sensitive to multipath propagation conditions than FM.

For the second generation cellular systems based on the TIA standard IS-54 that are currently being deployed, the performance in the presence of fading is an issue of major interest. In part, this is due to the fact that the standard specifies the transmitter signaling, and leaves the implementation of the receiver to the individual equipment manufacturers. A major outstanding issue is what kind of equalization is required and what should be the operating value of the signal-to-noise ratio. The answers to these questions will determine network factors affecting the capacity such as the cluster size in a frequency reuse pattern.

The other part of the uncertainty stems from the variations in the propagation environment, such as dense urban, urban, suburban, etc. No standard can be optimized to cover all possible environments. Rather, some engineering compromises have to be made. For instance, regarding the major issue of equalization, the IS-54 standard calls for the equalizer to work with delays up to 40 μs, although in several measurements performed in North America and Europe, significant components with delays up to 100 μs were recorded.

In order to propose or assess the potential performance of any standard, extensive sets of measurements are required. They should be taken both in typical and atypical mobile radio environments, and should provide sufficient information to predict system performance. In the case of the IS-54 standard, besides the carrier-to-interference ratio (C/I), the temporal distribution of the multipath powers should be measured as well, i.e., the impulse responses of the fading channel should be recorded and analyzed.

Temporal distributions of multipath delays and their associated powers were measured for the first time in New York City by Young and Lacy in 1950 [1]. In the early 1970's, more extensive measurement campaigns were undertaken in the San Francisco area by Turin [2] and in New York City by Cox [3]–[7]. However, in spite of these pioneering works, few measurements in North America were reported since then, until the measurements in four U.S. cities [7] were commissioned by the TIA in 1988, in order to support the IS-54 standard specification[1].

In Europe, on the contrary, although the first measurements appear not to have been reported until 1982 [8], numerous measurement campaigns were undertaken throughout the 1980's [9]–[20]. Most of these were performed in order to set the specifications for the European wide-band TDMA standard (GSM). Much attention was paid to the mountainous areas in Europe (especially Switzerland), and the standard calls for the equalization of excess delays up to 15μs.

In this paper, we report on a set of measurements performed in Toronto and the vicinity in order to assess the potential performance of the IS-54 standard in an area with a large cellular market. Typical results were sought, i.e., five of the

Manuscript received January 14, 1993; revised April 21, 1993 and November 24, 1993. This research was supported in part by a contract from Bell Mobility Cellular, and in part by a grant from the Information Technology Research Center of Ontario, ITRC.

E. S. Sousa is with the Department of Electrical and Computer Engineering, University of Toronto, Toronto, Canada M5S 1A4.

V. M. Jovanović was with the Department of Electrical and Computer Engineering, University of Toronto, Toronto, Canada M5S 1A4. He is now with Bell Mobility Cellular, Etobicoke, Ontario, Canada.

C. Daigneault was with Bell Mobility Cellular, Etobicoke, Ontario, Canada. He is now with Telesystem Financial Corporation, Quebec, Canada.

IEEE Log Number 9403809.

[1] We note, however, that an extensive set of delay spread measurements appears to have been performed in support of work leading to a CDMA proposal [21].

busiest cells were surveyed, without any bias towards the worst case locations and results. The results are expected to be useful to predict performance in other similar environments, for instance in most large cities in the eastern and central parts of North America.

Our measurements were motivated by the fact that the TDMA community appears to be operating under the assumption that much larger delay spreads and much larger delays than reported in most of the previous measurements are typical. For instance, some recent contributions to the TIA 45 Committee were based on the assumptions that *rms* delay spreads up to 60 μs would be common. This was one of the main reasons to report the results of this investigation.

The paper is organized as follows. Data collection procedures and the processing algorithm (*thresholding*) are described in Section II. Statistical results are presented in Section III, and in Section IV, the effects of shadowing and antenna sectorization are discussed. The main conclusions are summarized in Section V.

II. Data Collection and Processing

The measurement method is essentially the same as the one introduced by Cox [3] and involves transmitting a BPSK signal modulated by a maximal-length PN sequence and using a *sliding* correlator quadrature (I&Q) receiver. The actual apparatus is a modification of a system used previously in propagation measurements for some microcellular urban and indoor radio channels, described in [25]. The only differences come from the use of a 10 MHz, 511 b long PN sequence, which was phase-modulating the carrier at 910 MHz. This resulted in a temporal resolution of 0.1 μs, with an unambiguous delay span of 51.1 μs. The carrier and PN sequence clock frequencies were phased-locked to rubidium frequency standards so that the phases of the multipath echo components could be evaluated as well.

During the measurements, the transmitting omnidirectional antenna was placed on the existing base stations, near the existing cellular antennas. The cell-site building heights were between 18 and 28 floors. The receiver was mounted in a van, which was driven throughout the cells, along preassigned routes (*runs*). A typical *run* spanned one street within the cell, and the successive measurements were spaced by 30–100 m, depending on the size of the cell, resulting in 50–100 measurements per *run*. Uniform spacing was ensured by a distance measuring wheel mounted on the van.

Five existing cells were extensively scanned: two in downtown Toronto (cell radii 1 km), two in the suburbs (2 km) and one at the outskirts of the city (4 km). The last cell could be considered as a mixture of typical rural environment (north part) and suburban (south part of the cell).

To avoid the inclination towards the worst case locations and other possible operator-induced biases, operators were instructed to stop the van completely and take the measurement, regardless of what the signal at the particular location looked like. Each time, three waveforms were recorded. The quadrature signals were sampled four times per resolution chip, i.e., with the equivalent sampling frequency of 40 MHz,

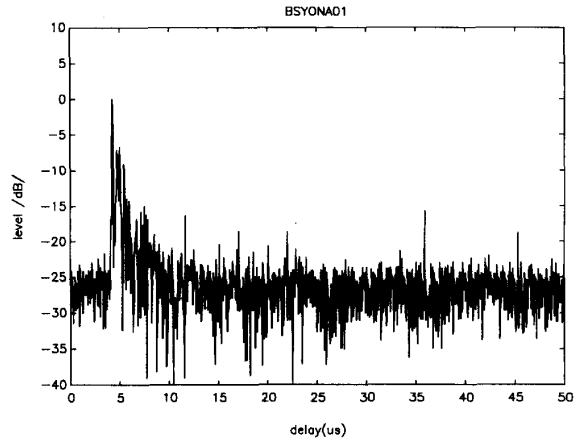

Fig. 1. Noisy delay profile for the measurement BSYONA01 taken at the intersection of Yonge and Front Streets.

resulting in 2044 complex samples per impulse response record. A typical delay profile, i.e., the magnitude of the received complex impulse response, obtained in such a manner is given in Fig. 1. This particular measurement was taken at the southeast corner of the intersection of Yonge and Front Streets, in the heart of downtown Toronto, in a cell with 1 km radius.

As Fig. 1 demonstrates, collected data has to be processed in order to eliminate the effects of noise and extract the valid echoes (*thresholding*). Unlike the measuring apparatus itself, *thresholding* procedures have not been discussed much in the past, although it is known that different algorithms can result in significantly different results on basically the same data [7].

In the first step of the technique used in the present analysis, for each record such as the one in Fig. 1, we want to estimate the level of background thermal noise, assumed to be Gaussian. The amplitude of this noise is Rayleigh distributed. We note that there is a significant probability that it would either considerably exceed or fall considerably below the mean noise value, due to the nature of the Rayleigh distribution. Nevertheless, if all 2044 samples were due to the noise, the noise variance σ_N^2 could have been estimated as one-half of the mean square value of the sample amplitudes. It is easy to verify that the variance of such an estimate would be very small, i.e., this estimate would be almost perfect for the present application. The valid echoes (and impulsive interference that is likely to appear in such measurements due to man-made noise), however, can significantly distort the mean value because of their comparatively very large power.

In order to mitigate the effects of the few very large data points (typically, valid echoes were found to appear in less than 5% of them) in our algorithm, σ_N^2 was evaluated based on the median of the samples. With no interference, the amplitude is Rayleigh distributed and the probability that the amplitude exceeds some level ζ is given by

$$P = \exp\left(-\frac{\zeta^2}{2\sigma_N^2}\right). \tag{1}$$

The estimated median level σ_m can be found by setting $\zeta = \sigma_m$, and by equating (1) with 0.5, so that

$$\sigma_N = \sigma_m / \sqrt{\ln 4} \approx 0.85\,\sigma_m. \tag{2}$$

The thermal noise standard deviation is thus 1.4 dB below the median in the absence of interference. We note that the confidence limits for the median level estimation are known to be somewhat larger than for the mean level estimation, but the difference is still negligible for the present purpose. Detailed analysis can be carried out following the procedures outlined in [31, Ch. 14].

The robustness of such an estimate with respect to the few very large data points can be verified from (1) as well. For instance, if these are present in, e.g., 10% of the samples, and are certain to be large with respect to σ_N, the median σ_m can be found from (1) by setting $P = 0.9 \cdot 0.5$; thus, 10% of the points with very large amplitudes would change the estimate of σ_N by only about 0.6 dB, no matter how large they actually are.

In contrast to most of the previous measurements where a fixed threshold appears to have been used, here we want to set the threshold to achieve a constant false alarm rate (CFAR) independently of the signal-to-noise ratio. The CFAR method is well known and widely used in radar, and requires the threshold to be set to $\zeta = \eta \cdot \sigma_N$, where ζ is a constant as shown below. From (1), we find the probability that the noise exceeds the threshold in any given sample without the echo (i.e., the false alarm probability per sample) to be

$$P_f = \exp\left(-\eta^2/2\right). \tag{3}$$

In the analysis of previous measurements, the false alarm probabilities involved with the thresholding were not specified for the most part, except in [7], where false alarm probability of 10^{-2} was chosen for the lowest signals expected to be processed. In those measurements, however, the number of samples per delay profile was 100, corresponding to approximately one false alarm in the delay profile with the minimum signal level, and rapid decrease with increasing the signal-to-noise ratio (SNR). Since in our CFAR scheme the false alarm rate is approximately the same independently of the SNR, we chose to have one false alarm per 100 recorded delay profiles, which corresponds to a false alarm probability of approximately 5×10^{-6}.

From (3), for $P_f = 5 \times 10^{-6}$, we would have to take $\eta \approx 4.94$, i.e., about 14 dB. For the data in Fig. 1, however, the median σ_m is found to be at the level of -27.7 dB, so that σ_N from (2) is approximately -29 dB, with respect to the maximum amplitude in the delay profile. The threshold would then be set at a relative level of -14 dB, and most of the echoes that are easily identified in Fig. 1 would not be detected as such, in spite of the relatively large level. Quantitatively, this can be verified from the miss probability which can be expressed in terms of Marcum's Q-function [24, p. 585] as

$$P_m = 1 - Q\left(\sqrt{SNR_k}, \eta\right). \tag{4}$$

The signal-to-noise ratio SNR_k of an echo in the k-th bin is defined as a_k^2/σ_N^2, where a_k is the amplitude of the multipath echo component in that bin.

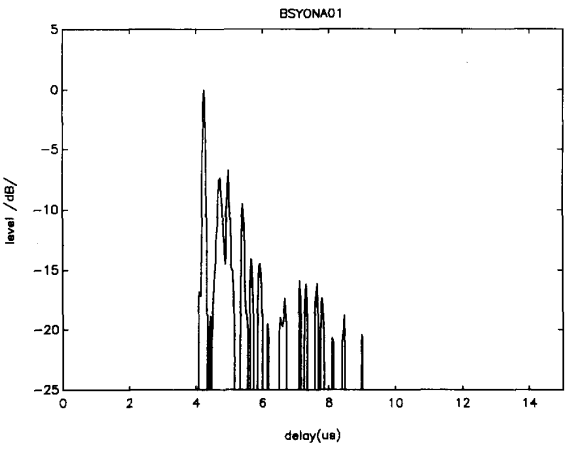

Fig. 2. Detected delay profile for the measurement BSYONA01 after the thresholding.

The CFAR thresholding algorithm can be easily improved in this case based on the fact that, although two consecutive quarter-chip spaced samples in the delay profile are highly correlated if the echo is present, two successive noise samples at the output of the sliding correlator are practically uncorrelated. The large noise samples are thus likely to be present in just one bin, while the samples containing the valid echoes will occupy at least two successive bins with high probability. Furthermore, since three delay profiles were recorded at each location, it is very unlikely that the large noise samples will be present at the same delay in all three records, or in two out of three records, etc. Several combinations of these two criteria were tested, which performed about the same with respect to the thermal noise. With respect to the impulse noise, the best algorithm turned out to be the one where a data point is declared to contain a valid echo only if the following two conditions were fulfilled simultaneously:

a) the threshold was exceeded at that point in all three recorded delay profiles;

b) at least one of the neighboring points satisfys a).

For each such point, the amplitude and the phase of the component were then evaluated as the means of the corresponding values in the three delay profiles.

For this algorithm, in the Appendix we show that the false alarm probability can be approximated by

$$P_{FA} \approx 2\left(P_f^3\right)^2 \approx 2\exp(-3\eta^2). \tag{5}$$

From (5), in order to have $P_{FA} = 5 \times 10^{-6}$, the threshold should be set at $\eta = 2.07$ times the estimated noise level σ_N, i.e., 6.3 dB above σ_N (or 4.9 dB above the median signal level σ_m).

As for the miss probability, with the parameter η set at approximately 2, at least three data points would be above the threshold for $SNR = 10$ dB. The probability of missing a valid echo can thus be upper-bounded by

$$P_M \leq 1 - \left((1 - P_m)^3\right)^2 \approx 6P_m, \tag{6}$$

provided that P_m in (4) satisfies $P_m \ll 1$.

Fig. 3. Downtown Toronto street map.

With $\eta = 2.07$, the miss probability P_M can be evaluated from (6) for any signal-to-noise ratio SNR. For instance, for $SNR = 15$ dB, a miss probability $P_M \leq 7 \times 10^{-4}$ is obtained. Since the noise level σ_N was below -29 dB with respect to the largest echo component in a typical measurement like that in Fig. 1, thus we conclude that on the average only one in a thousand echoes with amplitude larger than -15 dB, with respect to the largest echo, will not be detected. The delay profile obtained following the procedure outlined above is given in Fig. 2. We note that all the apparent echoes with delays larger than 15 μs in Fig. 1 were determined to be due to the noise. The resulting processed delay profile is shown in Fig. 2 where we have truncated the time scale, since there are no echoes with delays greater than 15 μs.

III. Results

In total, 2576 delay profiles were collected in 38 runs scanning five cells, as described in Section II. Approximately

35% of the measurements were taken in two urban cells, and the rest in three suburban ones. In one cell, approximately 400 measurements were taken with the 60° directional antenn in five runs transversing the same trajectories as the corresponding runs with the omnidirectional antenna.

The delay profile in Fig. 2 was quite typical for the results obtained in the high rise urban areas in downtown Toronto. The actual locations of the receiver and transmitter for this particular measurement are shown on the map in Fig. 3.

The location was on the border of the cell area (the designed cell radius was 1 km). In the figure, only the southeastern part of the cell is given, as most echoes would come from the high-rise buildings in this area (much fewer potential large reflectors exist east of Yonge Street). The largest delay in Fig. 2 is found to be at about 9 μs, and the shortest is at approximately 4 μs, corresponding to a path length of 1200 m. Potential loci of reflectors with various delays form an ellipse (assuming no multiple reflections), also shown in Fig. 3. The channel response in the spectral domain, obtained via the Fourier transform of the complex delay profile, is depicted in Fig. 4.

That the results presented in Fig. 2 (and Fig. 4) were typical for the data obtained in the whole run northbound along Yonge Street can be verified most easily from the contour plot of the delay profiles, given in Fig. 5. This plot can be viewed as an array of the delay profiles (normalized to the unity power), arranged horizontally as they were taken along the run.

Similar plots have been recently used in [21]; these plots appear to be very illustrative since the main component and numerous farther away echoes can be traced as the van travels throughout the cell. We found them to be very helpful in identifying the major reflectors along the route.

For each measured delay profile, several characteristic parameters were evaluated. The one used most widely so far is the *rms* delay spread, defined as the power-weighted second central moment of the component delays. Mathematically, since the delay profile in this case can be written as

$$a(t) = \sum_{k=1}^{2044} a_k \cdot e^{j\phi_k} \delta(t - \tau_k), \tag{7}$$

where a_k, ϕ_k and τ_k are the amplitude, phase and delay, respectively, of the k-th component in the delay profile, the *rms* delay spread σ_τ is given by

$$\sigma_\tau^2 = \sum_{k=1}^{2044} \frac{a_k^2}{P_t} (\tau_k - \tau_a)^2, \tag{8}$$

where P_t is the total power in the delay profile given by

$$P_t = \sum_{k=1}^{2044} a_k^2, \tag{9}$$

and τ_a is the power-weighted first moment of the echo delays

$$\tau_a = \sum_{k=1}^{2044} \frac{a_k^2}{P_t} \tau_k. \tag{10}$$

The distribution of the *rms* delay spreads (with vehicle stopped) obtained in this measurement campaign is given in Fig. 6. Plots are given separately for urban and suburban cells because a considerable variation was observed in these two environments.

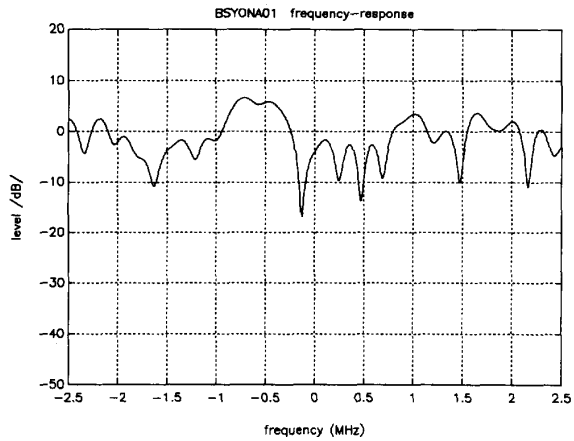

Fig. 4. Spectrum for the measurement BSYONA01.

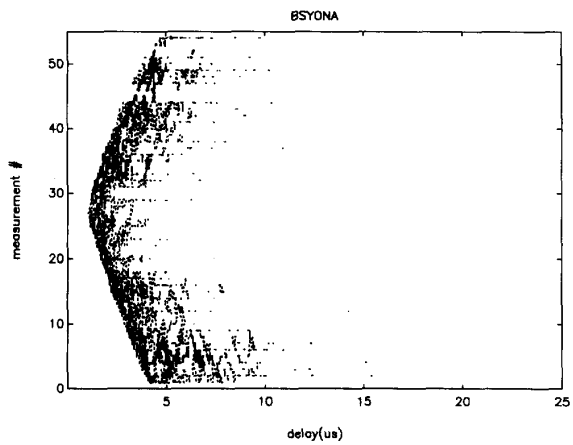

Fig. 5. Contour plot of the normalized delay profiles taken in the run BSYONA (Yonge Street).

We note that the *rms* delay spreads obtained in our measurements are somewhat smaller than what is often considered to be typical in urban environments [27]. For instance, we found the mean delay spread in urban areas to be 0.73 μs, while in [27] a typical value[2] is indicated as 1.3 μs. Our results for the median values, however, appear to compare well with the more recent results in [17, Fig. 8] for urban areas, and with the median for combined urban/suburban measurements in [19, Fig. 9] which were based on a larger number of samples[3].

In effect, the results given in Fig. 6 and in Table I compare favorably (i.e., are within a factor of less than two) with

[2]It appears that the values given in [27] were based mostly on the early results obtained by Cox and Leck [5] in New York City that were later corroborated by Bajwa and Parsons in Liverpool, UK [9]. However, in [17, p. 455], it was argued that the sample sizes in both measurements were around 100, which might not be sufficient.

[3]Fig. 9 in [19] is very similar to our results, except in the region below 5%. Higher probabilities of larger spreads are possibly due to the *local worst case* sampling applied in [19].

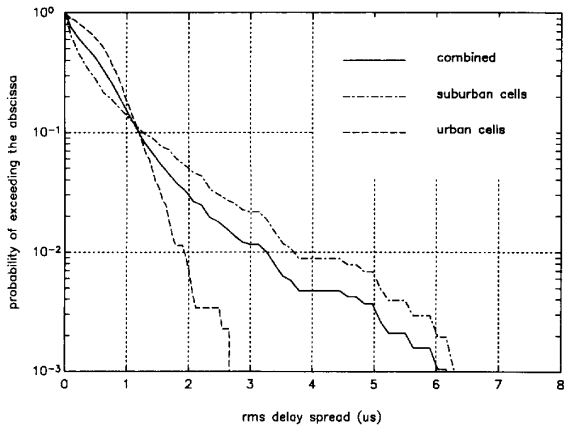

Fig. 6. Distribution of the measured *rms* delay spreads.

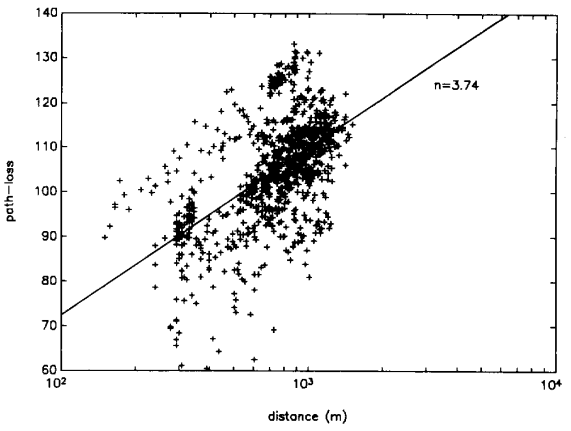

Fig. 7. Scatter plot of the path loss versus distance in urban cells.

TABLE I
AVERAGES OF THE *rms* DELAY SPREAD IN VARIOUS ENVIRONMENTS

	mean	median
urban	0.73	0.71
suburban	0.59	0.31
combined	0.66	0.48

almost all the previous measurements [5], [9], [10], [17]–[19], [26], except for some performed in very mountainous areas in Europe, such as the Swiss Alps [11], [15] and Norway [20]. Notable differences exist only with respect to the results obtained in the four U.S. cities [28] by the same authors as in [19], where a median *rms* delay spread of more than 2 μs was reported in essentially nonmountainous areas, with 1% probability of having *rms* delay spreads larger than 15 μs [28, Fig. 11].

It is interesting to note that urban and suburban/rural cells exhibit quite different variability in *rms* delay spreads. This can be verified in Fig. 6 and also in Table I, by noticing the almost two-fold difference between the median and the mean in suburban areas. This difference stems from the nature of these two environments. In urban cells, typically an almost continuous array of multipath components with decaying strengths can be observed up to excess delays of about 5 μs, with very few echoes with excess delays larger than 10 μs, as in Fig. 5. Although numerous, these echoes can not create extremely large *rms* delay spreads, and the results up to 3 μs are typical.

The absence of long delays, which would induce larger spreads and increase selectivity, can probably be explained by the fact that the same large reflectors in the vicinity that cause small delay echoes act as effective obstacles to the potential far away multipath components. This point can be further verified from Fig. 7 which shows a scatter plot of the path loss versus distance for data collected in urban cells.

In the same plot, the best linear fit is also shown. No specific reference distance nor reference path loss have been used [19], but the best linear regression curve turned out to have a path loss of 72.5 dB at 100 m distance, while in [19] a reference loss of 71.9 dB was proposed for the same distance. From Fig. 7, we see that the path loss exponent $n = 3.8$ is obtained for the best fit, additionally indicating that the paths in urban cells were quite heavily obstructed[4].

In the suburban/rural cells, on the contrary, due to the smaller number of potential reflectors, the multipath components tend to be much less numerous in general. Quite often, just two or three multipath components could be resolved, resulting in smaller *rms* spreads in general. However, a combination of existing large reflectors (hills, large buildings) and large *open* spaces sporadically gives rise to far away echoes with considerable amplitudes, sometimes yielding significant *rms* spreads. Thus, although the average *rms* delay spreads are smaller than in urban cells, the maximal values are considerably larger, ranging up to 7μs.

The longest echo in this set of measurements was found in one of these suburban cells, located Highway 401, the busiest highway in the Toronto area. Its absolute delay was 33 μs, and the excess delay was 28 μs, but this is not likely to affect the system performance, as the amplitude of that component was only -17 dB with respect to the strongest one.

Since the performance of a narrow-band digital system depends both on the delays and amplitudes of the multipath components, it is very difficult to relate the SNR or bit-error-probability to one single parameter of the delay profile. Although very handy for comparison purposes, the *rms* delay spread is no exception in that respect, because neither the quadratic weighting of the excess delays, nor the linear weighting of the powers in the components would be too illustrative for digital modulation schemes. For instance, a component with a relative level -20 dB and excess delay of 100 μs would have approximately the same contribution to the total *rms* delay spread as a 10 μs delay component with a power equal to the power of the largest component. Since the -20 dB component would hardly effect the performance, it is quite obvious that some form of nonlinear power weighting would be preferable.

[4]For distances 100 m to 1 km, path loss exponents are usually smaller. Exponents near 4 are characteristic in heavily shadowed, dense urban areas [19].

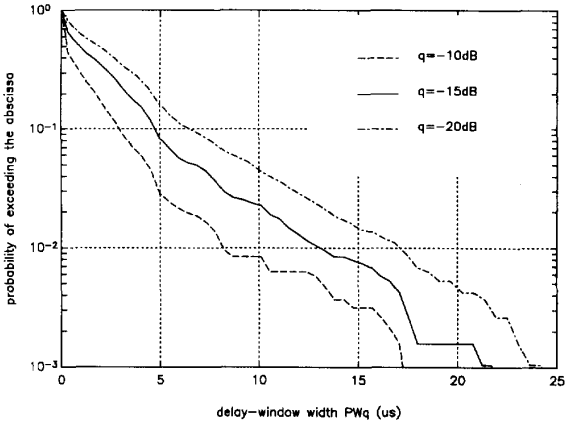

Fig. 8. Profile width parameter PWq distribution for $q = -10$, -15 and -20 dB, all cells combined.

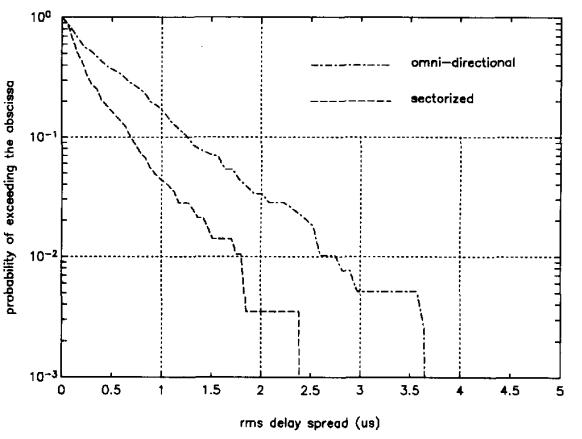

Fig. 9. Distribution of the *rms* delay spreads with the omnidirectional and sectorized antennas.

Although several parameters have been proposed so far in order to better reflect the performance of the equalized digital system on a given delay profile [29], here we chose to show a very simple parameter, the *profile-width (PWq)*. For a given level $q < 1$, it is defined as the maximum excess delay among all components with a normalized power level above q, and has also been used in [17], [19], [26], [28].

The parameter PWq is quite useful for discussing the nonequalized system performance. For instance, following the conventional wisdom that an equalizer is not needed if all the significant multipath components are within 10% of the symbol period [22], from Fig. 8 we see that the equalizer would not be needed in about 90% of the Toronto locations (slightly more if *insignificant* is defined as -20 dB with respect to the largest component, slightly less if the limit is assumed to be -10 dB). Analogously, if the equalizer is assumed to be mandatory for spreads larger than 20% of the symbol period, then we find that such situations exists in about 3% of the observed locations. Furthermore, based on Fig. 8, we could conclude that the TIA requirement for the equalizer to handle delays up to 40 μs would be much over-specified for an area like Toronto. In our measurements, excess delays of more than 20 μs would have to be equalized only in about 0.1% of the locations surveyed.

IV. Sectorization and Shadowing Effects

In one of the suburban cells, close to one of the busiest intersections in the Toronto area (Highways 401 and 427), the measurements were repeated using the existing cellular system antenna (60° beamwidth tilted antenna ALP6011). Since it fully illuminated the area to be surveyed and yet illuminated much fewer reflectors outside that area than the omnidirectional one, it was expected that the delay spreads would decrease.

Indeed, the *rms* delay spreads were found to decrease by about 30%, as shown in Fig. 9. This happened in all runs, except in the run along Eglinton Avenue, where the worst results had more than two times larger spreads with sectorized than with the omnidirectional antenna (data collected in that run are not included in Fig. 9). The largest *rms* delay spread (8.6 μs) in the whole campaign was also recorded there.

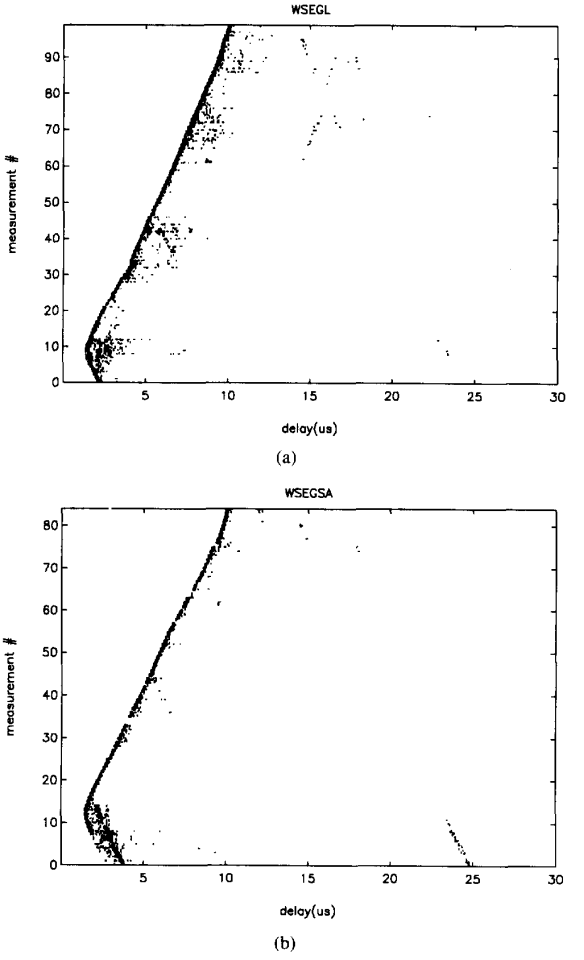

Fig. 10. Contour plot of the power delay profiles within the run along Eglinton Avenue: (a) omnidirectional antenna, (b) sectored antenna.

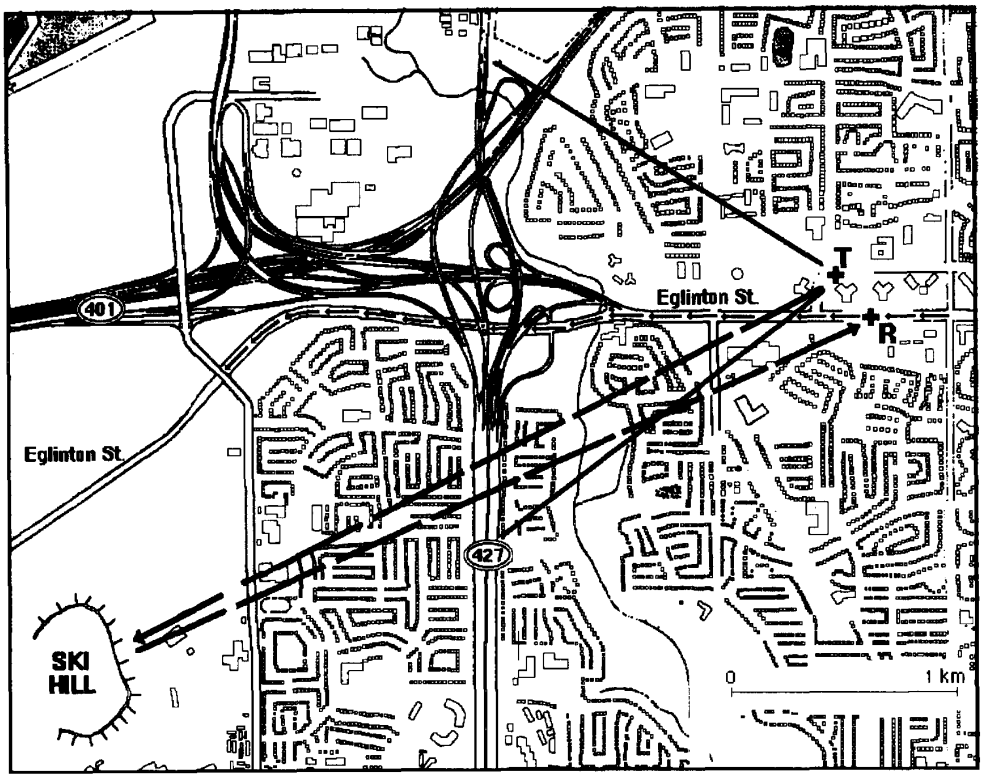

Fig. 11. Widdicombe cell.

Upon carefully inspecting the data, it was found that practically all the delay spreads decreased considerably, except for the first 15 results in the run, which were taken very *close* to the cell site. This can be verified from the contour plots given in Fig. 10.

From Fig. 10 we see that most of the echoes have really disappeared when the sectored antenna was utilized. However, the far away echoes with excess delays of about 22 μs became very pronounced, resulting in a large increase in the delay spreads. If we examine Fig. 11, where the west part of the Widdicombe cell is shown, it can be seen that the large echoes with the excess delay of about 22 μs are coming from the hilly region around Ski Hill, which happens to be the main source of long echoes in this cell. Furthermore, it can be verified that these same echoes also existed in the measurements done with the omnidirectional antenna, but were relatively much weaker. Upon inspecting the amplitudes of the detected components, the absolute level of long delay echoes was found to be about the same in both cases[5]. The absolute level of the direct components, however, was reduced by about 15 dB with the sectored antenna. This artificial shadowing effect is understandable when we note in Fig. 11 that it was just before these locations that the van crossed the sector border. Thus, the signal was attenuated because of the lower antenna gain and heavy shadowing by the base-station building itself.

From this example, we clearly see that even with small receiver-transmitter range, comparatively far away echoes are always possible in the presence of a large reflector, if only the main signal path becomes heavily obstructed. With larger cell radii, i.e., larger possible ranges, this same effect would produce larger absolute delays. If scaled to a cell radius of 4 km, instead of 2 km, this same example would result in the delay of 45 μs, for the radius of 8 km the delays would be 90 μs, etc. Furthermore, assuming the excess delay to be held constant, the relative power of the far away echoes will typically *increase* with increasing cell size, i.e., with an increase in receiver-transmitter range. This can be deduced from the fact that for a constant excess path length, the *relative* differences in the path lengths decrease as the direct path length increases. For a more elaborate discussion on this, see [30].

We note that the increase of the delay spreads with distance has been verified experimentally in [9] (high correlation was found between the *rms* delay spread and average delay, the latter parameter being closely related to the transmitter-receiver distance). Similarly, in [29], high correlation between the *rms* delay spread and the total path loss was demonstrated, which takes into account both the distance and shadowing effects.

[5]This is reasonable since the higher antenna gain was compensated for by the smaller transmitter power (the power was reduced from 10 W to 5 W for the sectored antenna), and by slanting (the hilly region was within the azimuth illuminated by the sectored antenna). Since this area was the main source of echoes, however, we note that in other five sectors the *rms* spread is likely to decrease for even more than 30%, but this should be verified experimentally.

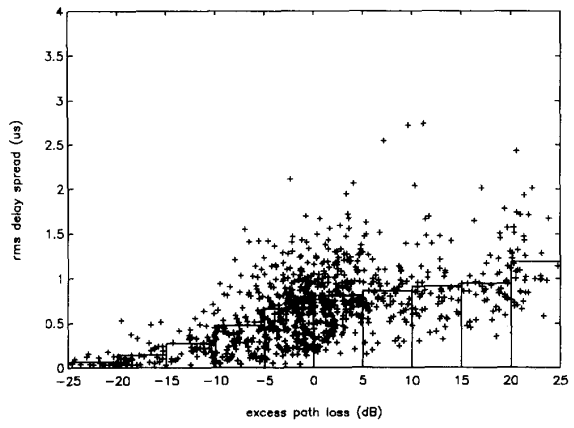

Fig. 12. Scatter plot of the *rms* delay spreads versus excess path loss in urban cells. Staircase curve represents the averages in the corresponding intervals.

In order to isolate these two effects, we calculated *rms* delay spread as a function of the excess path loss, which was obtained by subtracting the regression line in Fig. 7 from the corresponding path loss for each measured point. Thus, a positive excess path loss corresponds to higher than average shadowing, and vice versa for negative values.

The results in Fig. 12 show almost a ten-fold increase in the mean *rms* delay spreads when the excess path loss changes from -25 dB to 25 dB (heavy shadowing).

V. Conclusions

In the present measurements, we found that the urban cells are characterized by many multipath components but generally with excess delays up to 5 μs, yielding *rms* delay spreads up to 3 μs. Smaller mean delay spreads were found in suburban cells, but the variability appears to be much larger, resulting in delay spreads up to 7 μs. The multipath components in suburban areas, in general, tend to be less numerous, but echoes with excess delays up to 28 μs were recorded.

A sectorized antenna with 60° beamwidth was found to reduce the *rms* delay spreads by about 30% with respect to the omnidirectional one, in most cases. It is also possible for the delay spread to increase under rare cases of heavy shadowing. Further measurements would be needed in order to definitively confirm this result, as our experiment was performed in just one sector. If confirmed, it may be significant, since most previous measurements utilized omnidirectional antennae.

We have also found that an equalizer would not be needed in about 90%, and would be necessary in about 3%, of the measured locations. When required, however, the delay span that has to be equalized is less than 20 μs in all but 0.1% of the locations.

In general, our results show that the Toronto area exhibits smaller delay spreads than expected after similar measurements which were taken in four U.S. cities [28]. The smaller delay spreads obtained here are partly attributed to the essentially flat Toronto area, but also to the fact that the measurements were taken in real, existing cells. This resulted in smaller link distances and smaller shadowing than may be the case in a noncellular environment. Our results, however, appear to compare rather favorably with most of the measurements performed before and after [28], except for some results obtained in very mountainous areas in Europe.

Based on the example in Eglinton Avenue, we have shown that it would be possible to find very large delay spreads in Toronto as well (appropriately scaled down to account for the smaller cell size), but such situations would be atypical, and could be avoided or diminished by cellular engineering techniques (sectorization, careful selection of antenna patterns and pointing angles, and in some instances by introduction of new cells). In view of the results of our measurements, it appears that the long delay problem is not prevalent in an area such as Toronto.

On the other hand, dense urban areas like downtown Toronto will suffer from problems with short delays which lead to relatively flat fading. Unless a large fading margin is employed, the equalizers appear to be quite ineffective in these situations. However, systems with large fading margins are inefficient. It might be argued that the problem is similar to the one in present analog FM systems which are in the same sense also inefficient; but a digital system with large fading margins is much more so, because of the sharp thresholds inherent to digital modulations with powerful FEC and voice coding. It is our feeling that some other techniques, such as antenna diversity or fast intracell handoff, should be considered in order to circumvent this problem.

Although in view of our results we feel that the long delays problem was probably somewhat overemphasized in the past, we would like to add that delays longer than the equalizer's span will always arise in atypical cases. If sufficiently strong, they can result in outage, in spite of the high resultant signal level. Thus, the introduction of the digital TDMA systems would require a redefinition of coverage area: at least in some cases both C/I ratios and delay profiles would have to be taken into account.

Appendix

Here, we derive the false alarm probability per sample for the CFAR algorithm defined in Section II. We assume that the signal is not present in any of the 2044 temporal bins. The probability that any particular sample exceeds the threshold is denoted by P. The threshold crossings are independent, and a (false) echo appears only if the threshold is exceeded in at least two consecutive bins.

At first sight, the false alarm probability will not be constant for all samples—it will obviously be somewhat smaller for the very first and the very last one in the delay profile. However, due to the circular correlations involved in the sliding correlator system, these two bins are physically neighboring, i.e., an echo with the delay equal to the PN waveform period would have an apparent delay zero. If we define the first and the last bin to be neighboring as well, the false alarm probabilities will be stationary.

The false alarm probability P_{FA} can now be evaluated algebraically by enumerating all the possible cases, but the procedure would be tedious. An alternative approach is to

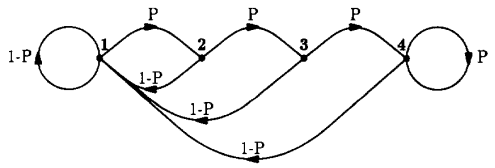

Fig. 13. Markov chain for the processing algorithm.

describe this sequential processing algorithm by a Markov chain, as in Fig. 13.

In Fig. 13, state **1** corresponds to the case when no crossings were detected, and state **2** to the case when a single threshold crossing occurred. No alarms will be generated in either of these states. State **3**, however, can be reached only after two consecutive crossings: each time when the algorithm enters state **3**, two points will be declared to belong to the delay profile. Similarly, state **4** then corresponds to the situation when one or more additional crossings were detected after the two initial ones; each time when the algorithm happens to be in this state, one additional point will be declared to belong to the delay profile.

For the Markov chain in Fig. 13, it is easy to construct the transition matrix **A** [32]

$$\mathbf{A} = \begin{Vmatrix} 1-P & P & 0 & 0 \\ 1-P & 0 & P & 0 \\ 1-P & 0 & 0 & P \\ 1-P & 0 & 0 & P \end{Vmatrix}. \tag{11}$$

The steady state probabilities p_j that the system will be in the j-th state can be evaluated following the methods indicated in [32]. With the aid of (11), we have

$$p_j = \begin{cases} P^{j-1}(1-P) & , \quad 1 \le j \le 3 \\ P^3 & , \quad j = 4 \end{cases}. \tag{12}$$

Since state **3** results in two false alarms, and state **4** results in one false alarm, the false alarm probability P_{FA} per sample will be

$$P_{FA} = 2p_3 + p_4 = 2P^2 - P^3. \tag{13}$$

If $P \ll 1$, then the second term in (13) can be neglected, i.e.,

$$P_{FA} \approx 2P^2. \tag{14}$$

In the algorithm, the probability P actually corresponds to the event where the thresholds are crossed simultaneously in three independent delay profiles. The crossing probability for one is given by P_f defined in (3), so that $P = P_f^3$, and if this is substituted into (14), (5) immediately follows.

ACKNOWLEDGMENT

We acknowledge the collaboration of the Communications Research Center (CRC), Department of Communications, Ottawa, in performing these measurements. We would especially like to thank Dr. Robert Bultitude, who developed the equipment and measurement techniques. Numerous discussions with him were very helpful. Additional thanks are due to R. Hahn of CRC, for his dedicated hard work during the ten days of the measurement campaign. We also acknowledge the contribution of P. Melancon of CRC, R. Lepage of Bell Mobility Cellular, and S. Tsui, S. Kandala, H. Yanikomeroglu, and the late Prof. J. L. Yen of the University of Toronto.

REFERENCES

[1] W. R. Young and L. Y. Lacy, "Echoes in transmission at 450 megacycles from land-to-car radio units," *Proc. IRE*, vol. 38, no. 3, pp. 255–258, Mar. 1950.
[2] G. L. Turin, F. D. Clapp, T. L. Jonhston, S. B. Fine and D. Lavry, "A statistical model of urban multipath propagation," *IEEE Trans. Veh. Technol.*, vol. VT-21, no. 1, pp. 1–9, Feb. 1972.
[3] D. C. Cox, "Delay Doppler characteristics of multipath propagation at 910 MHz in a suburban mobile radio environment," *IEEE Trans. Antenn. Propagat.*, vol. AP-20, no. 5, pp. 625–635, Sept. 1972.
[4] D. Cox, "910 MHz urban mobile radio propagation: Multipath characteristics in New York City," *IEEE Trans. Commun.*, vol. COM-21, no. 11, pp. 1188–1194, Nov. 1973.
[5] D. C. Cox and R. C. Leck, "Distributions of multipath delay spread and average excess delay for 910 MHz urban mobile radio paths," *IEEE Trans. Antenn. Propagat.*, vol. AP-23, no. 2, pp. 206–213, Mar. 1975.
[6] ——, "Correlation bandwidth and delay spread multipath propagation statistics for 910 MHz urban mobile radio channels," *IEEE Trans. Commun.*, vol. COM-23, no. 11, pp. 1271–1280, Nov. 1975.
[7] T. S. Rappaport, "900-MHz multipath propagation measurements for U.S. digital cellular radiotelephone," CTIA Digital Cellular Panel, Final Rep., Feb. 1989, App. I.
[8] A. Bajwa and J. Parsons, "Small area characterization of UHF urban and suburban mobile radio propagation," *IEE Proc.*, Part F, vol. 129, no. 2, pp. 102–109, Apr. 1982.
[9] ——, "Large area characterization of urban UHF multipath propagation and its relevance to the performance bounds of mobile radio systems," *IEE Proc.*, Part F, vol. 132, no. 2, pp. 99–108, Apr. 1985.
[10] J. V. Rees, "Measurements of the wide-band radio channel characteristics for rural, residential and suburban areas," *IEEE Trans. Veh. Technol.*, vol. VT-36, no. 1, pp. 2–6, Feb. 1987.
[11] A. Zogg, "Multipath delay spread in a hilly region at 210 MHz," *IEEE Trans. Veh. Technol.*, vol. VT-36, no. 4, pp. 184–187, Nov. 1987.
[12] P. W. Huish and E. Gurdenli, "Radio channel measurements and predictions for future mobile radio systems," *British Telecom Techn. J.*, vol. 6, no. 1, pp. 43–53, Jan. 1988.
[13] R. W. Lorentz, K. Low, M. Weber, P. Kartaschoff, P. Merki and J. P. Weck, "Excess delay power profiles measured in mountainous terrain," *Alta Frequenza*, vol. LVII, no. 2, pp. 57–64, Feb. 1988.
[14] E. Damosso, "Wide-band propagation measurements at 900 MHz," *Alta Frequenza*, vol. LVII, no. 2, pp. 65–74, Feb. 1988.
[15] J. P. de Weck, P. Merki and R. W. Lorenz, "Power delay profiles measured in mountainous terrain," in *Proc. 38th IEEE Veh. Technol. Conf.*, Philadelphia, PA, June 1988, pp. 105–112.
[16] A. J. Levy, J. P. Rossi, J. P. Barbot and J. Martin, "An improved channel sounding technique applied to wideband mobile 900 MHz propagation measurements," in *Proc. 40th IEEE Veh. Technol. Conf.*, Orlando, FL, May 1990, pp. 513–519.
[17] A. M. D. Turkmani, J. D. Parsons and D. A. Demery, "Measurement and modeling of wideband mobile radio channel at 900 MHz," *IEE Proc.*, Part I, vol. 138, no. 5, pp. 447–457, Oct. 1991.
[18] A. J. Levy and J. C. Bic and J. P. Rossi, "High selectivity occurrence of 900 MHz urban mobile radio channel," *Electron Lett.*, vol. 27, no. 24, pp. 2256–2257, Nov. 1991.
[19] S. Y. Seidel, T. S. Rappaport, S. Jain, M. L. Lord and R. Singh, "Path loss, scattering, and multipath delay statistics in four European cities for digital cellular and microcellular radiotelephone," *IEEE Trans. Veh. Technol.*, vol. 40, pp. 721–730, Nov. 1991.
[20] R. H. Raekken, H. Langaas, G. Lovnes and S. E. Paulsen, "Wideband impulse response measurements at 900 MHz and 1.7 GHz," in *Proc. GLOBECOM'91*, Phoenix, AZ, Dec. 1991, pp. 36.6.1–5.
[21] J. Shapira, "Channel characteristics for land cellular radio, and their system implications," *IEEE Antenn. Propagat. Mag.*, vol. 34, no. 4, pp. 7–16, Aug. 1992.
[22] J. G. Proakis, "Report on adaptive equalization requirements," CTIA Digital Cellular Panel, Final Rep., Feb. 1989, App. IV.
[23] ——, *Digital Communications*. New York: McGraw-Hill, 1983.
[24] M. Schwartz, W. R. Bennett and S. Stein, *Communication Systems and Techniques*. New York: McGraw-Hill, 1966.
[25] R. J. C. Bultitude, S. A. Mahmoud and W. A. Sullivan, "A comparison of indoor radio propagation characteristics at 900 MHz and 1.75 GHz," *IEEE J. Select. Areas Commun.*, vol. 7, pp. 20–30, Jan. 1989.

[26] R. J. C. Bultitude and G. K. Bedal, "Propagation characteristics on microcellular urban mobile radio channels at 910 MHz," *IEEE J. Select. Areas Commun.*, vol. 7, no. 1, pp. 31–39, Jan. 1989.
[27] W. C. Y. Lee, *Mobile Communications Engineering*. New York: McGraw-Hill, 1982.
[28] T. S. Rappaport, S. Y. Seidel and R. Singh, "900-MHz multipath propagation measurements for U.S. digital cellular radiotelephone," *IEEE Trans. Veh. Technol.*, vol. 39, pp. 132–139, May 1990.
[29] J. E. Berg, J. Ruprecht, J. P. Weck and A. Mattsson, "Specular reflections from high rise buildings in 900 MHz cellular systems," in *Proc. IEEE Veh. Technol. Conf.*, St. Louis, MO, May 1991, pp. 594–599.
[30] P. F. Driessen, "Measured propagation characteristics of 900 MHz mobile radio channels in mountainous terrain," in *Proc. 40th IEEE Veh. Technol. Conf.*, Orlando, FL, May 1990, pp. 603–609.
[31] M. G. Kendall and A. Stuart, *The Advanced Theory of Statistics*. London, UK: C. Griffin & Co., 1967.
[32] J. Kemeny and J. Snell, *Finite Markov Chains*. Princeton: Van Nostrand, 1960.

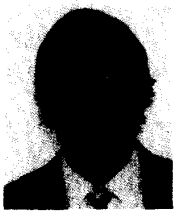

Elvino S. Sousa (S'80–M'86) was born in the Azores (Portugal), on December 28, 1956. He received the B.A.Sc. degree in engineering science, and the M.A.Sc. degree in electrical engineering from the University of Toronto in 1980 and 1982, respectively, and the Ph.D. degree in electrical engineering from the University of Southern California in 1985.

Since 1986, he has been with the Department of Electrical Engineering at the University of Toronto where he is presently an Associate Professor. Since 1986, he has been a Natural Sciences and Engineering Research Council of Canada (NSERC) University Research Fellow. He has performed research in the areas of packet radio networks, spread spectrum systems, mobile communications, and indoor wireless communications. At the University of Toronto, he has taught graduate courses in error-correcting codes and mobile communications. He has given various lectures and short courses on mobile communications throughout the world and is the Technical Program Chairman for PIMRC '95.

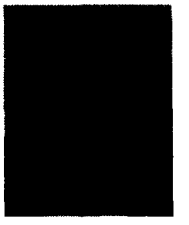

Vladan M. Jovanović (S'82–M'85) was born in Belgrade, Serbia, Yugoslavia. He received the B.S., M.S. and Ph.D. degrees in electrical engineering in 1981, 1985 and 1988, respectively, all from the University of Belgrade, Yugoslavia.

In 1981, he joined IMTEL—Institute of Microwave Techniques and Electronics, Belgrade, where he led several research and development projects in the field of spread spectrum. From May 1991 to February 1993, he was a Research Associate with the University of Toronto, Toronto, Canada, where he was involved in the studies of spread spectrum synchronization and multipath fading channels. He is now with Bell Mobility Cellular, Etobicoke, Canada, and is engaged in the RF technology planning. He has published articles in the areas of spread spectrum, error correction coding, efficient modulations, synchronization, fading channel characterization, etc.

Christian Daigneault (M'90) received the B.Sc. in electrical engineering from Université de Sherbrooke, Canada in 1986.

He is a Manager of Engineering, Wireless Communications Group with Telesystem Financial Corporation (TFC), the merchant bank of Canadian holding National Telesystem. Prior to joining TFC, he was Manager of R. F. Technology Planning with Bell Mobility Cellular.

Mr. Daigneault is a member of the Ordre des Ingénieurs du Québec.